Modeling free-surface solitary waves with SPH

Balázs Tóth

Department of Hydraulic and Water Resources Engineering, Budapest University of Technology and Economics, Budapest, Hungary

Abstract

A weakly compressible SPH solver is presented and applied to simulate free-surface solitary waves generated in a dam-break experiment. Wave propagation speeds are compared with the exact solutions of the Korteweg-de Vries (KdV) equation as a first order theory and a second order approximation investigated in the literature. Test cases are constructed based on the measurement layouts of a dam-break experiment. Free surface shapes of different simulation cases are compared with the KdV-shapes. The simulation results show good agreement with the second order approximation of solitary wave propagation speeds.

Keywords: Soliton, Solitary wave, Free-surface flow, Smoothed Particle Hydrodynamics

1. Introduction

The first known observation of a solitary wave was reported by Scott Russell in 1834 [1]. He studied the behaviour of the solitary waves in laboratory while the first theoretical model explaining them appeared in 1895 by Korteweg and de Vries [2]. The idea of the Korteweg-de Vries (KdV) theory is based on slightly dispersive shallow water waves whose dispersion is balanced by nonlinear effects so that the wave preserves its amplitude and shape during the propagation on arbitrary distances. The exact solution of the KdV equation describes the shape and propagation speed of a soliton. Although the KdV theory can be considered a first order approximation and its solution describes real solitary waves well, higher order approximations can also be constituted. In [3] Halász introduced an arbitrarily high order iterative, successive approximation model that reproduces the KdV theory in the first iteration step, however, the higher order investigation requires

numerical approach.
Smoothed Particle Hydrodynamics (SPH) is a meshless Lagrangian numerical scheme firstly published by R.A. Gingold and J.J. Monaghan [4] and independently by L. Lucy [5] in 1977. In the beginning SPH was applied in the field of astrophysics, then the first attempts on modeling fluid flows motivated by coastal engineering problems was published by J.J. Monaghan in 1994 [6] and [7]. Later the investigation of the dynamics of Scott Russel's Solitary wave generator with SPH has been carried out by the same author in 2000 [8]. Different aspects of free-surface waves in SPH were rigorously investigated, like turbulence modeling of breaking waves by R.A. Dalrymple and B.D. Rogers [9]. Standing and regular waves were modelled by Antuono et al. in [10] and the damping of viscous gravity waves in SPH were validated to analytical solutions by M. Antuono and A. Colagrossi [11]. Solitary waves over non-uniform bottoms and wave-splitting mechanics were investigated by Li et al. [12] and S. De Chowdhury and S.A. Sannasiraj in [13].
During the past two decades, owing to its attractive properties and prominent capabilities in modeling free surface flows, SPH became one of the most popular particle based numerical schemes in many different areas of engineering applications, like modeling coastal waves or tsunamies.

The paper is organized as follows. In the next section a short overview of free-surface solitary wave models is presented, then the governing equations of fluid dynamics and a novel SPH-based parallel solver is introduced. After the specification of the investigated test cases in Section 6 the results are compared with the first and second order wave propagation velocities of the literature and KdV soliton shapes in the last two sections.

2. Solitary waves

The zeroth order approximation of solitary wave propagation can be described by the linear wave propagation equation, and the wave speed in shallow water is given by the formula:

$$c_0 = \sqrt{gH} \tag{1}$$

where g is the gravitational acceleration and H is the depth of the ambient water. This relation gives a rough approximation on solitary wave propagation but neglects some particular features of the phenomenon like the actual

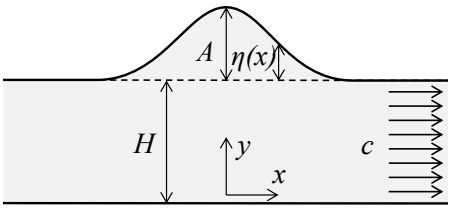

Figure 1: Notations of the solitary wave: H is the ambient depth, c is the speed of the soliton, A is the amplitude and $\eta(x)$ is the shape of the surface.

amplitude and width of the wave and is valid only if $A << H$. The linear wave propagation equation has no solitary wave solutions.

The KdV equation

$$\frac{\partial \eta}{\partial t} + c\left[\frac{\partial \eta}{\partial x} + \frac{H^2}{6}\frac{\partial^3 \eta}{\partial x^3} + \frac{3}{2H}\frac{\partial \eta}{\partial x}\right] = 0, \tag{2}$$

is suitable for construction of free surface soliton shapes with different geometrical configurations. Here $\eta(x,t)$ denotes the surface elevation at a given location x. Figure 1 shows a soliton propagating from the right to the left with the corresponding notations. The exact solution of the KdV equation for a single free surface solitary wave is given by the shape of the wave

$$\eta(x) = Ach^{-2}(k(x-a)), \tag{3}$$

where A is the amplitude, a is the horizontal displacement of the soliton and

$$k = \sqrt{\frac{3A}{4H^3}} \tag{4}$$

is the effective wave number. The wave propagation speed related to the first order solitary wave solution is

$$c_1 = \sqrt{gH}\left(1 + \frac{A}{2H}\right). \tag{5}$$

The second order wave speed including the corrections described by Halász is given as

$$c_2 = \sqrt{gH}\left(1 + \frac{A}{2H} - \frac{3A^2}{20H^2}\right). \tag{6}$$

Halász [3] has shown that the second order approximation describes well the laboratory results for the solitary wave speed and that the third order theory differs only by a small amount that is usually not resolvable due to experimental uncertainty error.

3. Governing equations

In fluid mechanics, the Euler and the continuity equations are widely used together to describe inviscid fluid motion. In the Lagrangian frame of reference these partial differential equations are expressed in terms of material coordinates where the local and convective fluxes are wrapped in the Lagrangian total derivative

$$\frac{\mathrm{d}\Phi}{\mathrm{d}t} = \frac{\partial\Phi}{\partial t} + \mathbf{v}\nabla\Phi, \tag{7}$$

denoting an arbitrary scalar or vector field by Φ. By employing the differential operator (7) the inviscid hydrodynamic equations become

$$\begin{aligned} \frac{\mathrm{d}\mathbf{v}}{\mathrm{d}t} &= -\frac{1}{\rho}\nabla p + \mathbf{g}, \\ \frac{\mathrm{d}\rho}{\mathrm{d}t} &= -\rho\nabla\mathbf{v}, \end{aligned} \tag{8}$$

where $\mathbf{v}$, ρ, p, ν, $\mathbf{g}$ are the velocity, density, pressure, kinematic viscosity, and gravitational acceleration, respectively. For weakly compressible flows an additional state equation

$$p = p(\rho), \tag{9}$$

is required to define a constraint between pressure and density.
Although there exist numerous analytic solutions of restricted variants of the system (8) includeing the wave propagation equations shown before, the exact solution in the generic case is still unknown and usually approximated by suitable numerical methods. However, these approximating schemes often suffer from unfavourable numerical properties, whereupon their generality is often limited and possess restricted robustness and applicability. Considering laminar inviscid flows the difficulties of modeling complex turbulent hydrodynamic behaviour are avoided in the present work.

4. The numerical scheme

The meshless Lagrangian numerical scheme called Smoothed Particle Hydrodynamics (SPH) is a suitable numerical tool for solving the system of equations introduced in (8). The approximate solution provided by SPH is based on elementary fluid nodes, called particles, moving through space while carrying their own values of mass, density, pressure, velocity, etc. The discretisation method is based on the weighted interpolation of the fields at a given point using the neighbouring particles governed by the so-called smoothing kernel function $W(\mathbf{r}_i - \mathbf{r}_j, h)$ forming a discrete convolution [14]

$$\langle f \rangle_i = \sum_{j=1}^{N} V_j f_j W_{ij}, \tag{10}$$

where i denotes the particle of interest, j is a particle in the vicinity of i, $f_i = f(\mathbf{r}_i)$ is an arbitrary flow field at the position $\mathbf{r}_i$ of particle i, the kernel function $W_{ij} = W(\mathbf{r}_i - \mathbf{r}_j, h)$ with compact or infinite influence radius, h is called the smoothing length, V_j is the elementary volume assigned to particle j and N is the number of particles within the influence radius of W_{ij}. The discrete convolution (10) constructs an arbitrary flow field on a statistically uniform distribution of particles in space. In our calculations the renormalised Gaussian kernel function [15]

$$W_{ij} = \begin{cases} \frac{e^{-(r/h)^2} - C_0}{C_1} & \text{if } r < \delta \\ 0 & \text{otherwise,} \end{cases} \tag{11}$$

is adopted, where $r = |\mathbf{r}_i - \mathbf{r}_j|$, and the renormalisation constants are

$$\begin{aligned} C_0 &= e^{-(\delta/h)^2}, \\ C_1 &= \pi^{3/2} h^3 \left(1 - 10 C_0\right). \end{aligned} \tag{12}$$

In this case, the influence radius δ was chosen to be $3h$. Similarly to (10) the first order spatial differential operators

$$\begin{aligned} \left(\mathrm{grad} f\right)_{\mathbf{r}_i} &\approx \langle \nabla f \rangle_i = \sum_{j=1}^{N} V_j \left(f_j + f_i\right) \nabla_i W_{ij}, \\ \left(\mathrm{div} \mathbf{u}\right)_{\mathbf{r}_i} &\approx \langle \nabla \mathbf{u} \rangle_i = \sum_{j=1}^{N} V_j \left(\mathbf{u}_j - \mathbf{u}_i\right) \nabla_i W_{ij}, \end{aligned} \tag{13}$$

can be constructed by an arbitrary vector field marked by $\mathbf{u}$ [16].
It is a prevailing practice in the SPH scheme to preserve numerical stability by inserting numerical diffusive terms into the continuity and momentum equations. The latter behaves similarly to viscosity generally resulting in a spurious dissipation of kinetic energy of the flow [14], especially in case of shock waves [17]. Since free surface solitons are driven by inertial forces and show inviscid behaviour, the momentum diffusion (either physical on numerical) was ignored in the present work. Instead the numerical diffusive term for density in the continuity equation worked out by [15] and further improved by [18] was implemented. Based on the linear stability analysis by Antuono [19] the density diffusion became an efficient tool on damping numerical oscillations.
The compressibility, as another particular numerical property of standard SPH, was controlled by an appropriate weakly compressible equation of state assuming a barotropic fluid flow with linear relation between density and pressure [7]. The discretised hydrodynamic equations of the SPH scheme used through this paper are

$$\begin{cases} \dfrac{\mathrm{d}\rho_i}{\mathrm{d}t} = \rho_i \displaystyle\sum_j (\mathbf{v}_i - \mathbf{v}_j)\nabla_i W_{ij} V_j + \xi h c_s \sum_j \Psi_{ij} \nabla_i W_{ij} V_j, \\ \dfrac{\mathrm{d}\mathbf{u}_i}{\mathrm{d}t} = -\dfrac{1}{\rho_i} \displaystyle\sum_j (p_i + p_j)\nabla_i W_{ij} V_j + \dfrac{1}{\rho_i}\, \mathbf{f}_i, \\ p_i = c_s^2(\rho_i - \rho_0), \\ \dfrac{\mathrm{d}\mathbf{r}_i}{\mathrm{d}t} = \mathbf{v}_i, \end{cases} \tag{14}$$

where ρ_0 is the reference density, $\mathbf{f}$ is the sum of the external forces including gravity and c_s is the speed of acoustic wave (or 'sound') propagation. The second term on the right hand side of the continuity equation is the artificial density diffusion term, forming a model often referred as δSPH with the empirical coefficient $\xi = 0.1$, and

$$\Psi_{ij} = 2(\rho_i - \rho_j)\frac{\mathbf{r}_{ij}}{|\mathbf{r}_{ij}|^2} - \left[\langle\nabla\rho\rangle_i^L + \langle\nabla\rho\rangle_j^L\right]. \tag{15}$$

The second term on the right hand side with the renormalised density gradients $\langle\nabla\rho\rangle^L$ ensures mass conservation over the fluid domain including free

surface boundaries and it is calculated using the formula

$$\langle \nabla \rho \rangle_i^L = \sum_j (\rho_i - \rho_j) \mathbf{L}_i \nabla_i W_{ij} V_j,$$
$$\mathbf{L}_i = \left[\sum_j (\mathbf{r}_i - \mathbf{r}_j) \otimes \nabla_i W_{ij} V_j \right]^{-1}, \tag{16}$$

where $\otimes$ denotes tensor product. The renormalisation tensor $\mathbf{L}$ is responsible for the convergence of the discrete Laplacian in the vicinity of the fluid boundaries by correcting the numerical artifacts in the discrete gradient caused by kernel truncation.
To reduce computational cost, the weakly compressible models usually operate with moderate sound speed (in comparison to the physical one), but large enough to keep the maximum density deviation within a predefined range and separate inertial and acoustic waves. It is usually considered to be ten times larger than the typical velocity magnitude being present in the flow:

$$c_s = \frac{1}{M} \sqrt{gH}, \tag{17}$$

where $M = 10$ is the Mach number and H is the characteristic height of the problem, which is the ambient fluid depth in our case.

4.1. Boundary and initial conditions

A remarkable benefit of the SPH scheme (at least in modeling fluid flows) is the treatment of free surfaces of arbitrary shape as natural boundaries without any additional computational effort. Furthermore, if the fluid domain is simply connected the air can be entirely left out from the computational domain because of its constant pressure and negligible density compared to water. Note that in case of complex flows such as breaking waves (see more examples in [20]) the air phase might play an important role, thus it should not be ignored unconditionally. In the present work we modelled only the water phase.

In this work two different types of boundary conditions of SPH were applied. One of them formed the rigid boundaries of the channel wall and bottom, while the other one was a periodic boundary, which allows one to perform more general calculations in infinite domain.
Here periodic boundaries were essential by forming a 2δ width domain in

spanwise direction to approximate a planar flow with the three dimensional numerical solver described in the next section.
The models of solid boundaries in SPH have several fundamentally distinct variants with different assets and limitations [16]. In the present work a penalty force-based boundary condition was applied presented by Sun et al. in [21]. The boundary model is based on the Voigt model with ideal spring and viscous damping. We applied the particle-wall interaction forces (elastic and viscous) only in normal direction to achieve exact free-slip condition. A further benefit of the model is its computational efficiency due to the lack of additional wall-particles.

4.2. Integration

The system (14) can be solved by an arbitrary but stable numerical integration scheme. In the present work the second order predictor-corrector scheme was applied. In the first step the particles are temporarily advanced in time with a half-step $\Delta t/2$ (prediction):

$$\begin{aligned} \rho_i^{n+1/2} &= \rho_i^n + \frac{\Delta t}{2}\frac{\mathrm{d}\rho_i}{\mathrm{d}t}\bigg|_i^n, \\ \mathbf{v}_i^{n+1/2} &= \mathbf{v}_i^n + \frac{\Delta t}{2}\mathbf{a}_i^n, \\ \mathbf{r}_i^{n+1/2} &= \mathbf{r}_i^n + \frac{\Delta t}{2}\mathbf{v}_i^n. \end{aligned} \tag{18}$$

In the intermediate state the density derivatives, pressures, external and interparticle forces (or accelerations $\mathbf{a}_i$) of particles are evaluated. Using the new values, the particles are advanced in time with a full step (correction) from the original state [22]:

$$\begin{aligned} \rho_i^{n+1} &= \rho_i^n + \Delta t\frac{\mathrm{d}\rho_i}{\mathrm{d}t}\bigg|_i^{n+1/2}, \\ \mathbf{v}_i^{n+1} &= \mathbf{v}_i^n + \Delta t\mathbf{a}_i^{n+1/2}, \\ \mathbf{r}_i^{n+1} &= \mathbf{r}_i^n + \Delta t\mathbf{v}_i^{n+1/2}. \end{aligned} \tag{19}$$

To reduce the computational performance requirement while preserving numerical stability the time step size might be selected adaptively in each

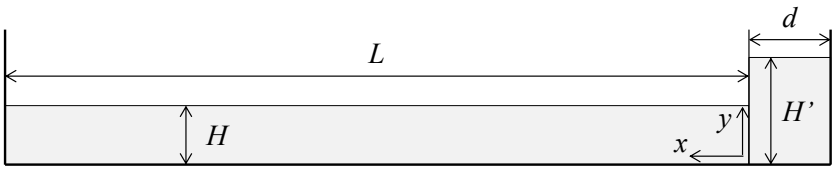

Figure 2: The whole channel layout ($L = 10$m, $d = 0.13$m, $H = 0.103$m and H' is 0.17m or 0.24m depending on the simulation case).

frame. In the current SPH model this was implemented using the Courant-Friedrichs-Lewy condition [7]:

$$\Delta t^{\text{new}} = CFL \cdot \min_i \left\{ \sqrt{\frac{h}{|\mathbf{a}_i|}}, \frac{h}{c_0 + h \max_j \left(\frac{\mathbf{v}_{ij}\mathbf{r}_{ij}}{|\mathbf{r}_{ij}|^2} \right)} \right\}, \tag{20}$$

where $CFL = 0.2$ and $\mathbf{v}_{ij} = \mathbf{v}_i - \mathbf{v}_j$.

5. Simulation tools

Since the three dimensional model requires large number of particles to resolve the fluid motion the simulations become computationally expensive. The favourable vectorisation properties of the explicit particle based methods allow the current and many other solvers (like [23], [24] and [25]) to exploit the abilities of computationally powerful GPGPU's (General-Purpose Graphical Processing Unit) rendering the solutions through massively parallel calculations. To further reduce the computational time, the time-consuming data copies between host and device memory are minimised by transferring the partial results from the device only at predifined equidistant simulation-time intervals $t_s = 0.033$s. The presented SPH model was implemented in a novel three dimensional parallel fluid dynamics solver using GPGPU in C++ and CUDA.

6. Test cases

We have simulated the propagation of a single solitary wave in an infinitely wide channel, as appearing in a wet bed dam break experiment, reproducing the conditions investigated in [3]. Halász performed several measurements of single solitary waves in a channel layout introduced in Figure 2

with hydrostatic initial conditions. By removing the flat plate at the water column on the right hand side of the channel at instant $t_0 = 0$s, the collapse of the water column forms a solitary wave propagating from the right to the left. As Halász pointed out, a solitary wave travels through the channel without significant dissipation until it reaches the vertical wall at the end of the channel.

The performed simulations cover six independent configurations: three sizes of particle support radii, with two different initial water column heights. The influence radii of the particles, the initial water column height, and the number of particles for the different computations are summarised in Table 1. The average interparticle distance is given as

$$dx = \sqrt[3]{\frac{4\delta^3\pi}{3N}}, \tag{21}$$

where the average number of neighbours N was chosen to 70 in this work showing the mean interparticle distance $dx = 1.173h$.

7. Results and discussion

In the present work each calculation has been executed on a GTX 970 desktop GPU with 4 GB of device memory. The time and memory requirement of the computations varied between 36 and 180 hours while 0.6 and 3.8 GB's of GPU memory depending on the number particles used.

The evaluation of the propagation speed of the simulated solitary wave along the channel required a free surface tracking algorithm which reliably identifies the position of the wave peak in each investigated simulaton frame. Since in our case only the vertical positions need to be determined, we logged the highest particle's altitude above the uniform δ-sized grid laying on the plane of the channel bottom in each time instant. Due to the discrete convolution (10) the free surface boundary covering a set of particles is not sharp and need to be tuned carefully. Here the surface was shifted from the layer of the surface particles by the average interparticle distance dx.
The velocity series were calculated by applying a moving average filter to the raw position data with a filter size $\Delta t = 20t_s$ and the temporal derivative was calculated with a first order central finite differencing scheme. The smooth velocity data series was resampled on a uniform Δt-sized grid. By

Table 1: Summary of simulation cases

Case	$\delta[mm]$	$dx[mm]$	H/dx	$H'[m]$	Particles
a	2.5	0.678	151.9	0.17	$5.48M$
b	2.5	0.678	152.9	0.24	$5.54M$
c	3.75	1.02	101.0	0.17	$2.45M$
d	3.75	1.02	101.0	0.24	$2.47M$
e	5.0	1.36	75.7	0.17	$1.38M$
f	5.0	1.36	75.7	0.24	$1.39M$

means of the introduced procedure the velocity data was constructed in the 5m width window between 4m and 9m measured from the right hand side of the channel.

Implementing the channel layout introduced by [3] in the numerical model has two important advantages. On the one hand the calculation results are suitable for direct comparison with the measurements, on the other hand the velocity field below the solitary wave does not have to be prescribed by the initial conditions of the simulations. The main numerical drawback is that it is inevitable to update each particle in the entire tank in every simulated time step, however, the region of interest is small in comparison with the whole channel.

In Figure 3 we see the wave propagating speed-amplitude relations of the first and second order theories against our simulation results. For each point, the instantaneous amplitude and propagation speed were extracted from the reconstructed surface history to plot instantaneous normalized propagation speed against instantaneous relative amplitude.

It is visible that along the investigated section of the channel (from 4m to 9m) the solitary wave speed and amplitude diminished considerably, governed by a continuous dispersion. Nevertheless, the simulation results seem to more or less follow the line of the second order approximation, as if the solitary wave would be an ideal soliton in each time instant. Apparently, in all simulation cases, the second order theory is closer to the simulation results than the first order theory.

The effect of the resolution represented by the particle influence radius δ

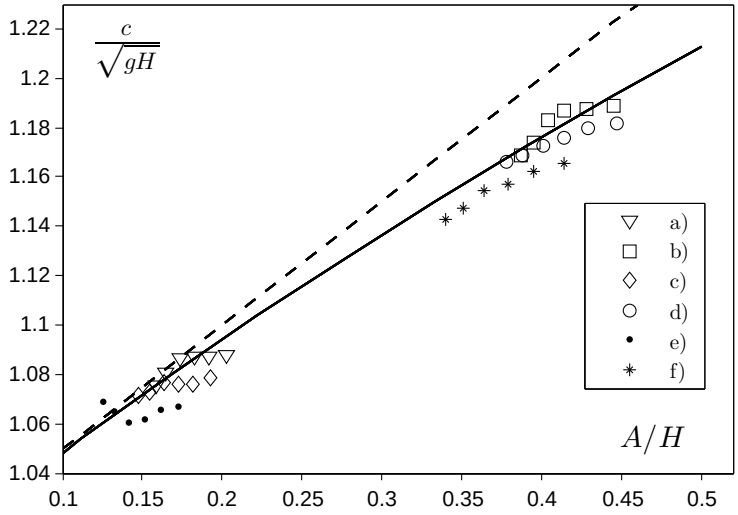

Figure 3: Dimensionless soliton wave speed as a function of dimensionless amplitude. Dashed and solid curves are the first and second order approximations respectively.

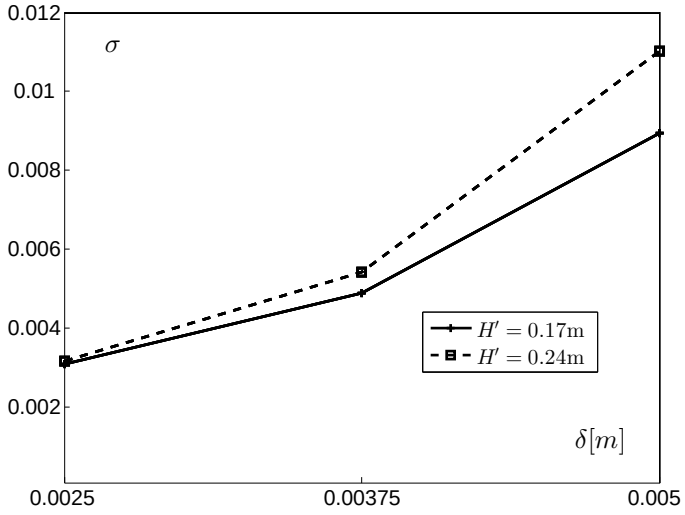

Figure 4: RMS of the deviation of the six simulation cases to the second order approximation.

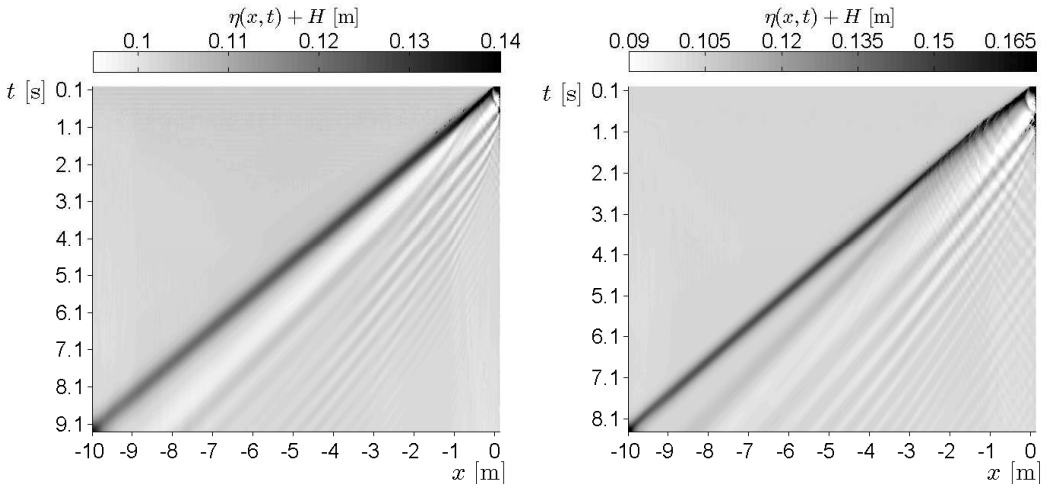

Figure 5: Free surface history of case a) (left) and b) (right)

was investigated through the root mean sqaure (RMS) error

$$\sigma_{II} = \sqrt{\frac{1}{N}\frac{1}{c_0^2}\sum_{k=1}^{N}\left(c_k - c_2(A_k/H)\right)^2} \tag{22}$$

of the simulation results c_k compared to the second order theory $c_2(A_k/H)$ given by (6). As Figure 4 shows, reducing the influence radius δ, the values of the RMS σ are decreasing considerably.

7.1. Surface evolution

The evolution of the free surface in time along the channel during the solitary wave propagation as captured by the simulations with the finest resolution is presented in the space-time plots of Figure 5. The dark diagonal stripes are indicating the solitary waves travelling at nearly constant speed through the channel followed by a significantly slower wave pattern with small amplitudes compared to the solitary wave. This wave pattern is observable in the channel during measurements as well. Furthermore a marked depression is present behind the solitary wave in case a) while this phenomenon does not occur in case b). Note that the noisy surface immediately after the launch of the wave in case b) was caused by the slight break of the wave peak along the first few meters in the simulations, reported in laboratory measurements as well.

7.2. Solitary wave shape

Besides the solitary wave propagation speed the shape of the free surface was compared to the first order soliton shapes obtained from the analytical solution of the KdV equation. The comparison is shown in Figure 6; the waves propagate from the right to the left. The exact solutions (3) were fitted to the given SPH results using the evaluated amplitudes and peak positions, defining together the effective wave number (4).

The wave shapes are in very good agreement with the exact solutions of the KdV equation even in case of coarser resolutions, apart from the depression, which appears close in the tail of the solitons with smaller amplitudes in case *a*), *c*) and *e*) likewise to Figure 5. The existence of this trailing depression has been verified experimentally for the transient flow investigated. For further details on the comparison of the waveform to experimental data see Appendix A.

8. Summary and Conclusions

In this work, water surface solitary wave formation and propagation have been investigated with a novel numerical fluid dynamics solver based on the Smoothed Particle Hydrodynamics scheme and the results have been compared with the first order analytical theory (KdV equation) and a second order approximation introduced by Halász in [3]. The simulation layouts of a dam break experiment were adopted from the measurements carried out by Halász.

The instantaneous dimensionless velocities and their corresponding amplitudes extracted from the simulations show that although significant dispersion occurs during the wave propagation, the velocity-amplitude relation follows the second order analytical approximation, also verified by the measurements in [3] within measurement uncertainty. The resolution dependency of the numerical model was also tested by three different particle support radii presenting the clear convergence to the second order approximation.

Solitary wave shapes provided by the numerical model were also compared with the closed-form analytical formula of the first order KdV-soliton. Our simulation results show very good agreement with the first order soliton shape even in case of coarser numerical resolutions for the leading edge and the peak shape. However, since the waves were generated in a numerical dam-break

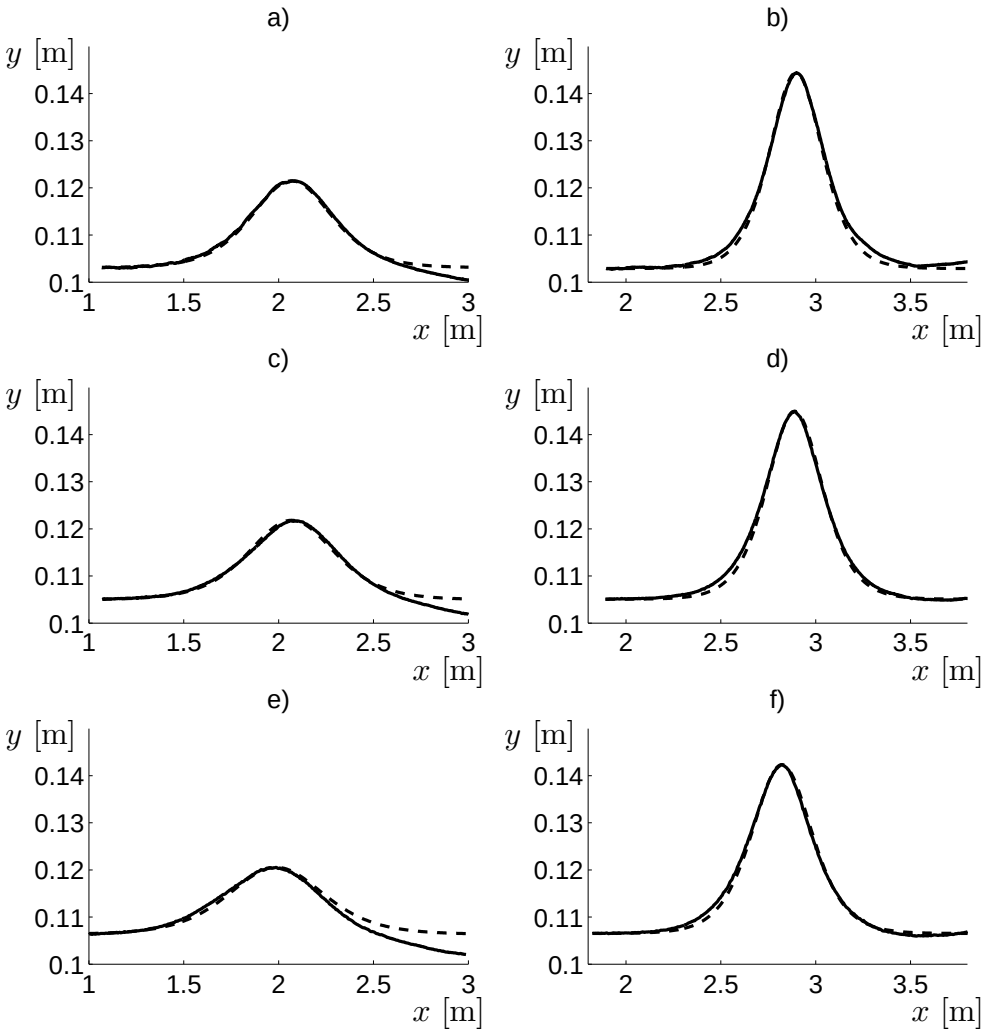

Figure 6: SPH soliton shapes (solid lines) compared with the exact solution of the KdV-equation (dashed lines) at the same time instant $t = 6.6$s.

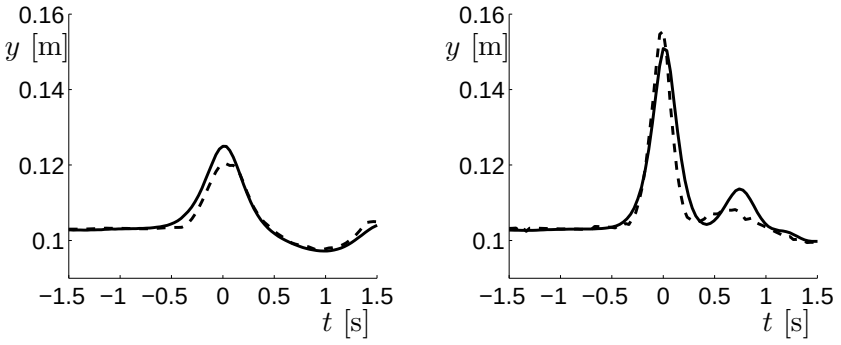

Figure A.7: Comparison of measurements (dashed lines) with SPH simulations (solid lines) in case of $H' = 0.17$m (right) and $H' = 0.24$m (left) at $x = 4$m.

experiment, the transient formation of the solitary wave also included trailing waves behind the developing soliton. In case of smaller solitary waves significant depressions (and consequently notable antisymmetries of the wave shapes) were observed behind the waves. We found that, if such transient flows should be modeled, these trailing waves found in the simulations cannot be verified by either the present first or the second order approximations, as these models describe only the propagation of a developed solitary wave. The verication of the presence of these trailing waves in our simulation results is shown by comparison with water height time-series extracted from our preliminary experimental measurements (see Appendix A) resulting in a good qualitative match in both investigated test cases.

9. Acknowledgement

The present investigation was professionally supported by Miklós Vincze and Zsolt Várhegyi through personal discussions. The measuerements were performed in the von Kármán Laboratory in the Institute of Physics of Eötvös Lóránd University, Hungary.

Appendix A.

Measurements focusing on the surface shapes were also carried out based on the same geometry (and, in fact, the very same experimental wave tank) investigated in [3]. During the measurements, the surface level was observed

in fixed positions along the channel then the extracted time-series were compared with the corresponding simulation results. In Figure A.7 typical time-series are shown for both initial configurations ($H' = 0.17$m and 0.24m). In both cases the time series were extracted at $x = 4$m and shifted in time to set the wave peak to $t = 0$s. The significant depression, also seen in Figure 5 and 6 is visible in the tail of the 'small' solitary wave. In a subsequent work a detailed investigation is planned to be presented about the surface shape of the solitary waves in measurements and SPH simulations.

References

[1] P. Drazin, R. Johnson, Solitons: An Introduction, Cambridge Computer Science Texts, Cambridge University Press, 1989.

[2] D. J. Korteweg, G. de Vries, On the change of form of long waves advancing in a rectangular canal, and on a new type of long stationary waves, Philosophical Magazine Series 5 39 (240) (1895) 422–443.

[3] G. B. Halász, Higher order corrections for shallow-water solitary waves: elementary derivation and experiments, European Journal of Physics 30 (2009) 1311–1323.

[4] R. A. Gingold, J. J. Monaghan, Smoothed particle hydrodynamics theory and application to non-spherical stars, Monthly Notices of the Royal Astronomical Society 181 (1977) 375–389.

[5] L. B. Lucy, A numerical approach to the testing of the fission hypothesis, Astronomical Journal 82 (1977) 1013–1024.

[6] J. J. Monaghan, Simulating Free Surface Flows with SPH, Journal of Computational Physics.

[7] J. J. Monaghan, A. Kos, Solitary waves on a Cretan beach, Journal of Waterway, Port, Coastal and Ocean Engineering 125 (3) (1999) 145–154.

[8] J. J. Monaghan, A. Kos, Scott Russell's wave generator, Physics of Fluids 622.

[9] R. A. Dalrymple, B. D. Rogers, Numerical modeling of water waves with the SPH method, Coastal Engineering 53 (2006) 141–147.

[10] M. Antuono, A. Colagrossi, S. Marrone, C. Lugni, Propagation of gravity waves through an SPH scheme with numerical diffusive terms, Computer Physics Communications 182 (4) (2011) 866–877.

[11] M. Antuono, A. Colagrossi, The damping of viscous gravity waves, Wave Motion 50 (2) (2013) 197–209.

[12] J. Li, H. Liu, K. Gong, S. Keat, S. Shao, Sph modeling of solitary wave fissions over uneven bottoms, Coastal Engineering 60 (2012) 261–275.

[13] S. D. Chowdhury, S. A. Sannasiraj, SPH Simulation of shallow water wave propagation, Ocean Engineering 60 (2013) 41–52.

[14] J. J. Monaghan, Smoothed particle hydrodynamics, Reports on Progress in Physics 68 (2005) 1–34. arXiv:0507472v1.

[15] D. Molteni, A. Colagrossi, A simple procedure to improve the pressure evaluation in hydrodynamic context using the SPH, Computer Physics Communications 180 (2009) 861–872.

[16] D. Violeau, Fluid Mechanics and the SPH Method, Oxford University Press, 2012.

[17] L. Cullen, W. Dehnen, Inviscid smoothed particle hydrodynamics, Monthly Notices of the Royal Astronomical Society 408 (2) (2010) 669–683. arXiv:1006.1524.

[18] M. Antuono, A. Colagrossi, S. Marrone, D. Molteni, Free-surface flows solved by means of SPH schemes with numerical diffusive terms, Computer Physics Communications 181 (3) (2010) 532–549.

[19] M. Antuono, A. Colagrossi, S. Marrone, Numerical diffusive terms in weakly-compressible SPH schemes, Computer Physics Communications 183 (12) (2012) 2570–2580.

[20] A. Colagrossi, M. Landrini, Numerical simulation of interfacial flows by smoothed particle hydrodynamics, Journal of Computational Physics 191 (2) (2003) 448–475.

[21] X. Sun, M. Sakai, Y. Yamada, Three-dimensional simulation of a solid-liquid flow by the DEM-SPH method, Journal of Computational Physics 248 (2013) 147–176.

[22] J. J. Monaghan, On the problem of penetration in particle methods, Journal of Computational Physics 82 (1) (1989) 1–15.

[23] A. Crespo, J. Domínguez, B. Rogers, M. Gómez-Gesteira, S. Longshaw, R. Canelas, R. Vacondio, A. Barreiro, O. García-Feal, DualSPHysics: Open-source parallel CFD solver based on Smoothed Particle Hydrodynamics (SPH), Computer Physics Communications 187 (2015) 204–216.

[24] J. Cercos-Pita, AQUAgpusph, a new free 3D SPH solver accelerated with OpenCL, Computer Physics Communications 192 (2015) 295–312.

[25] B. L. Wang, H. Liu, Application of SPH method on free surface flows on GPU, Journal of Hydrodynamics 22 (2010) 869–871.